

# Dynamics of the charged particles released from a Sun-grazing comet in the solar corona

ChuanPeng Hou<sup>1</sup>, JianSen He<sup>1\*</sup>, Lei Zhang<sup>2,3,1</sup>, Ying Wang<sup>1</sup>, and Die Duan<sup>1</sup>

<sup>1</sup>School of Earth and Space Sciences, Peking University, Beijing 100871, China;

<sup>2</sup>Qian Xuesen Laboratory of Space Technology, Beijing 100094, China;

<sup>3</sup>SIGMA Space Weather Group, National Space Sciences Center, Chinese Academy of Sciences, Beijing 100190, China

## Key Points:

- We find that charged dust particles released in the solar corona can be rebounded away from the sun by the magnetic mirror force, contributing to the formation of a dust-free zone close to the sun.
- We propose that the distortion of the cometary tail can be used to infer the topological change of the coronal magnetic field direction.
- We suggest that, compared with magnetic gradient and curvature drifts, the electric field drift dominates the perpendicular drift motion of cometary oxygen ions.

**Citation:** Hou, C. P., He, J. S., Zhang, L., Wang, Y. and Duan, D. (2021). Dynamics of the charged particles released from a Sun-grazing comet in the solar corona. *Earth Planet. Phys.*, 5(3), 232–238. <http://doi.org/10.26464/epp2021023>

**Abstract:** The sun-grazing comet C/2011 W3 (Lovejoy) showed a distorted, unconventional tail morphology near its perihelion ( $1.2R_s$ ). Based on the “Solar Corona and Inner Heliosphere” modeling result of the magnetic field and plasma dynamics in the solar corona, we use the Runge-Kutta method to simulate the moving trajectory of charged dust and ion particles released at different positions from the C/2011 W3 orbit. We find that the dust particles near the sun, which are subject to a strong magnetic Lorentz force, travel differently from their counterparts distant from the sun, where the latter are mainly affected by the solar gravitational force and radiation pressure. According to the simulation results, we propose that the magnetic mirror effect can rebound the charged dust particles back away from the sun and be regarded as one crucial cause of the dust-free zone formation. We find that ions mainly move along magnetic field lines at an acute angle to the comet’s direction of motion. The cometary ions’ movement direction was determined by the comet’s velocity and the coronal magnetic field, which are responsible for the C/2011 W3’s unique comet tail shape near perihelion. Additionally, the ion particles also experience perpendicular drift motion, mainly dominated by the electric field drift, which is similar to and can be used to approximate the solar wind’s transverse velocity at its source region.

**Keywords:** Sun-grazing comet; cometary tail; solar corona; solar wind; dust-free zone

## 1. Introduction

Sun-grazing comets commonly belong to the Kreutz family and their perihelia are about  $1\text{--}4R_s$  (Jones et al., 2018), thought to be fragments formed after a comet broke up (Sekanina and Chodas, 2007). With the launch of the Solar and Heliospheric Observatory (SOHO) in 1995 (Brueckner et al., 1995) and the advancement of space exploration, by 2016, people have discovered more than 2700 Kreutz comets and a few sun-skirting comets (Battams and Knight, 2017), the perihelia of which are about  $10R_s$  (Jones et al., 2018). Since sun-grazing comets can penetrate deep into the solar corona and experience extreme environments, observations of sun-grazing comets are of great significance for understanding the activity of comets, the features of the corona, and their inter-

actions.

The activity and material composition of comets can be obtained by multi-band spectral observation. Biesecker et al. (2002) studied the light curve of 141 sun-grazing comets observed by SOHO from 1996 to 1998 and found that the peak brightness of comets appears between  $7R_s$  and  $12R_s$  away from the solar center, which is possibly due to comet ruptures. Based on the spectral observations, useful information about comets can be obtained, such as nucleus sizes (Bemporad et al., 2005; McCauley et al., 2013), the gas release rate (McCauley et al., 2013) and the relative abundances of elements (Ciaravella et al., 2010; McCauley et al., 2013). In the ultraviolet band, hydrogen generated by photolysis of water scatters Ly $\alpha$  light. Giordano et al. (2015) compared the measurement results of Ly $\alpha$  band with Monte-Carlo simulation results to study the properties of the corona and solar wind (e.g. temperature, density, velocity). Raymond et al. (2018) estimated the properties of solar wind with a global magnetohydrodynamic (MHD) simulation. Based on the extreme ultraviolet images of C/2011 W3

Correspondence to: J. S. He, jshept@pku.edu.cn

Received 26 NOV 2020; Accepted 01 FEB 2021.

Accepted article online 16 MAR 2021.

©2021 by Earth and Planetary Physics.

(Lovejoy), McCauley et al. (2013) studied the tail striations at different spectral lines and suggested that these spectral lines correspond to a series of excited states of oxygen.

When approaching perihelion, comets release dust particles into the surrounding environment due to sublimation (Jewitt, 2012) and thermal fracture (Li J and Jewitt, 2013; Jewitt et al., 2013). These dust particles will undergo sublimation, decomposition, and ionization (Russell, 1929; Downs et al., 2013). Hence, Russell (1929) first proposed that there should be a region near the sun called the dust-free region, where all dust particles are ionized. At present, comet debris collected on Earth mainly consists of pyroxene and olivine (Jessberger et al., 2001). If the orbit of dust particles around the sun is assumed to be circular, then the boundary of the dust-free zone of pyroxene is  $5R_s$  (Mann et al., 2004). Considering that sun-grazing comets are mostly long-period comets in elliptical orbits with large eccentricity, Sekanina and Chodas (2012) suggested that the boundary of the dust-free zone should be at  $1.8R_s$ . Recent observations by Parker Solar Probe have found that the dust thermal emission intensity decreases within  $17R_s$ , which may be regarded as direct observational evidence of the dust-free zone (Howard et al., 2019). Mukai (1981) proposed that, due to the ionization, the surface potential of dust particles with diameters of 10 nm is  $+5 - +10$  V. Supposing that the dust particles are spherical with a density of  $3.5 \text{ g} \cdot \text{cm}^{-3}$ , then the charge-mass ratio of charged dust particles is  $10^{-5} \frac{e}{m_p}$ , where  $e$  is the electron charge and  $m_p$  is the proton mass (Meyer-Vernet et al., 2009; Czechowski and Mann, 2010; Ip and Yan TH, 2012). We propose that this kind of charged dust particle can be bounced by the magnetic mirror-type geometry during its approach to the sun in favor of the dust-free zone formation.

As a sun-grazing comet that survived through perihelion ( $1.2R_s$ ) (Sekanina and Chodas 2012), C/2011 W3 showed a distorted striation tail around the perihelion time (2011-12-16 00:17 UT). Downs et al. (2013) proposed that striations may be caused by the movement of charged particles along magnetic field lines and compared two coronal magnetic field models based on observations. Raymond et al. (2014) thought the striations reflect that C/2011 W3 might have passed through different magnetic flux tubes. The work of Downs et al. (2013) and McCauley et al. (2013) suggest that the comet tail of C/2011 W3 near perihelion may be mainly composed of a series of excited-state oxygen ions including  $O^{5+}$ . Oxygen ions (e.g.,  $O^{5+}$  and  $O^{6+}$ ) can undergo chemical reactions leading to the loss or gain of mass through photo- and impact ionizations in the solar corona and can be treated as separate fluid species in multi-fluid MHD modeling (Jia et al., 2014). After inspecting the projection and column densities, the multi-fluid simulation results show a dominance of  $O^{5+}$  and  $O^{6+}$  ions in the cometary tail, and they interpret the phenomenon of bright tail structure observed as oxygen ion lines in the extreme ultraviolet (EUV) band (Jia YD et al., 2014). However, the fluid-like treatment cannot disentangle the complex movements of oxygen ions being transported parallel and perpendicular to the magnetic field direction.

To better understand the formation of the dust-free zone and C/2011 W3's comet tail morphology, we simulate the movement

of C/2011 W3's tail particles (charged dust particles and  $O^{5+}$ ). Based on the simulation results, we propose a new mechanism for the formation of dust-free regions and explain the formation of the comet tail's morphology around perihelion. In the next section, we introduce the data and methods, followed by Section 3 where we show and discuss the simulation results, summarizing in Section 4.

## 2. Model Setup and Running

We use the fourth-order Runge-Kutta method to simulate the trajectory of ions and charged dust particles in the heliocentric co-rotation coordinate system. The fourth-order Runge-Kutta method, which has a global error on the order of  $O(\Delta t^4)$  with  $\Delta t$  being the time step, is often employed in modeling the dynamics of space particles. After setting the time step  $\Delta t$ , the initial position  $r_0$ , and the initial velocity  $v_0$  of the particles, their position and velocity along with the time can be determined.

Force analysis and calculation are crucial for the calculation of the particles' movement. For charged dust particles, we consider solar gravity, radiation pressure, Lorentz force and inertial force (see Equation (1)–(3)). We obtain the ratio of radiation pressure and solar gravity from Equation (4). For  $O^{5+}$  ions, the gyro-radius is small and the gyro-frequency is high, so in order to save calculation time, we use the guiding center approximation and calculate the position and velocity of the guiding center. Besides parallel motion, different types of perpendicular drift motion of the guiding center are shown in Equation (5)–(8) (Gordovskyy et al., 2010). The initial position and velocity of dust particles and  $O^{5+}$  ions are assumed to be the same as that of C/2011 W3, utilizing the asteroid ephemeris provided by NASA's Jet Propulsion Laboratory. The plasma and magnetic field data in the corona are needed to calculate forces and the ions' drift velocity. Here we use the modeling result from Solar Corona and Inner Heliosphere (SWMF/SC/IH) model provided by Community Coordinated Modeling Center (CCMC), and the time range is selected at the 2118th Carrington rotation (2011-12-13 14:40:50 UT–2012-01-09 22:35:54 UT). The inner boundary of the model is the top of the chromosphere, and the outer boundary is at  $24R_s$ . This model is based on the BATS-R-US MHD code. For the inner boundary conditions, the magnetic fields are based on a synoptic magnetogram (GONG/MDI), the temperature is 50000 K and the density is  $2 \times 10^{11} \text{ cm}^{-3}$ . The outer boundary conditions are set as extrapolation conditions for the supersonic and super-Alfvénic outflows.

$$\mathbf{F}_{\text{grav}} = -\frac{GMm\mathbf{r}}{r^3}, \quad (1)$$

$$\mathbf{F}_{\text{em}} = \frac{q}{m} (-\mathbf{V}_{\text{sw}} \times \mathbf{B} + \mathbf{V}_{\text{dust}} \times \mathbf{B}), \quad (2)$$

$$\mathbf{F}_{\text{rad}} = \frac{I_{\text{sc}} R_s^2 \pi \frac{d^2}{4} \mathbf{r}}{c r^2} = \frac{\pi I_{\text{sc}} R_s^2 d^2 \mathbf{r}}{4r^2 c} \quad (3)$$

where,  $G$  is the gravitational constant,  $M$  is the solar mass,  $q$  and  $m$  are the charge and mass of dust, respectively.  $\mathbf{r}$  represents the space position of dust particles,  $\mathbf{V}_{\text{sw}}$  and  $\mathbf{V}_{\text{dust}}$  respectively represent the velocities of solar wind and dust particles in the heliocentric co-rotation reference frame. Here, we assume the magnet-

ic frozen-in condition and have replaced the electric field  $\mathbf{E}'_{\text{sw}}$  with  $-\mathbf{V}_{\text{sw}} \times \mathbf{B}$ .  $I_{\text{sc}}$  is the solar constant ( $1366 \text{ W/m}^2$ ).  $R_s$  is the solar radius,  $c$  is light speed, and  $d$  represents the diameters of dust particles.

$$\beta = \frac{F_{\text{rad}}}{F_{\text{grav}}} = \frac{3\pi ER^3}{2GMcd\rho} \sim \frac{1}{d}. \quad (4)$$

In [Figure 1](#), the ratios of radiation pressure to gravity ( $\beta$ ) shows an anti-correlation with dust particle diameter, which is greater than  $1 \mu\text{m}$ . The radiation pressure is the pressure of solar radiation acting on the particle. [Dohananyi \(1978\)](#) added an effective factor of momentum transfer into Equation (4), and the value of  $\beta$  for the nano-dust grains is expected to be small ( $\sim 0.1$ ) ([Czechowski and Mann, 2010](#); [Ip and Yan TH, 2012](#)). As shown in [Figure 3a](#) and [3d](#), our results are not sensitive to  $\beta$  value. So, we set  $\beta$  equal to 0.1 for dust particle diameters less than  $1 \mu\text{m}$ , and calculate  $\beta$  using Equation (4) for dust particles with diameters greater than or equal to  $1 \mu\text{m}$ .

The governing equations for the guiding center of ions are expressed as:

$$\frac{d\mathbf{r}}{dt} = \mathbf{u} + v_{\parallel} \mathbf{b}, \quad (5)$$

$$\begin{aligned} \mathbf{u} = & \mathbf{u}_E + \frac{mv_{\parallel}^2}{qB} [\mathbf{b} \times (\mathbf{b} \cdot \nabla) \mathbf{b}] + \frac{mv_{\parallel}}{qB} [\mathbf{b} \times (\mathbf{u}_E \cdot \nabla) \mathbf{b}] \\ & + \frac{mv_{\parallel}}{qB} [\mathbf{b} \times (\mathbf{b} \cdot \nabla) \mathbf{u}_E] + \frac{m}{qB} [\mathbf{b} \times (\mathbf{u}_E \cdot \nabla) \mathbf{u}_E] \\ & + \frac{m\mu}{qB} [\mathbf{b} \times (\nabla B)] + \frac{\mathbf{F}_{\text{cent}}}{q} \times \mathbf{B}, \end{aligned} \quad (6)$$

$$\frac{dv_{\parallel}}{dt} = \frac{q}{m} \mathbf{E} \cdot \mathbf{b} - \mu (\mathbf{b} \cdot \nabla B) + v_{\parallel} \mathbf{u}_E \cdot ((\mathbf{b} \cdot \nabla) \mathbf{b}) + \mathbf{u}_E \cdot ((\mathbf{u}_E \cdot \nabla) \mathbf{b}), \quad (7)$$

$$\frac{d\mu}{dt} = 0, \quad (8)$$

where  $\mathbf{r}$  is the position of the ion's guiding center,  $\mathbf{u}$  is the velocity of the ion's guiding center,  $v_{\parallel}$  is the ion's parallel velocity,

$$\mathbf{b} = \frac{\mathbf{B}}{B}$$

is the direction of the magnetic field,

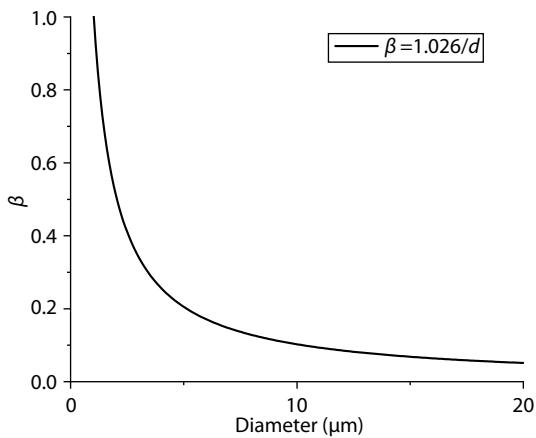


**Figure 1.** The relation between the ratio of solar radiation pressure to solar gravity ( $\beta$ ) and the diameter of dust particles.

$$\mathbf{u}_E = \frac{\mathbf{E} \times \mathbf{b}}{B}, \quad \mu = \frac{u_g^2}{2B}$$

is the magnetic moment,  $u_g$  is the cyclotron velocity of ions. The above set of equations has been used to study the dynamics of the electron's guiding center and electron acceleration associated with interchange magnetic reconnection in the solar corona ([Yang LP et al., 2014](#)).

In studies of particle motion within the planetary magnetosphere, the additional drift caused by inertial force is considered in the corotation coordinate system. When solving the azimuth drift velocity, Coriolis force and centrifugal force need to be considered separately ([Huang et al., 1988](#)). Considering the centrifugal force  $\mathbf{F}_{\text{cent}}$ , we add

$$\frac{\mathbf{F}_{\text{cent}}}{q} \times \mathbf{B}$$

to the right side of Equation (6). The angular velocity in the Coriolis force term is equivalent to the additional magnetic field  $\delta\mathbf{B}$ , and the magnetic field  $\mathbf{B}$  in the equation becomes  $\mathbf{B} + \delta\mathbf{B}$ . Since  $\delta\mathbf{B}$  introduced by the angular velocity of the sun is far less than  $\mathbf{B}$ , the contribution of the Coriolis force can be ignored.

### 3. Results and Discussion

#### 3.1 Dynamics of Charged Dust Particles

For charged dust particles, we choose 10 different positions before perihelion for C/2011 W3, as the dust ejection places in the time range of 22:00–22:45 UT on 2011-12-15. Each position is 5 minutes apart, and the distance range of the initial position is  $\sim 2.5R_s$ – $3.5R_s$ . The initial position and velocity of the dust particles at each position are set to those of C/2011 W3. We test the dust particles of three diameters (10 nm,  $1 \mu\text{m}$ , and  $10 \mu\text{m}$ ) at each position. The  $\beta$  for 10 nm dust particles are set to 0.1, and the ratio  $\beta$  for dust particles of  $1 \mu\text{m}$  and  $10 \mu\text{m}$  is calculated with Equation (4).

In [Figure 2](#), particles of 10 nm are mainly controlled by the Lorentz force (see [Figure 3a, 3d](#)) after leaving C/2011 W3, and the particles gyrate when moving along the magnetic field line. With decreasing heliocentric distance and increasing magnetic field, the particles are subjected to the magnetic mirror force. As a consequence, the parallel velocity decreases and the vertical velocity increases, finally reversing at a certain magnetic mirror point. For dust particles with diameters of  $1 \mu\text{m}$  and  $10 \mu\text{m}$ , due to their small charge-to-mass ratio, they are mainly controlled by gravity (see [Figure 3b–3c, 3e–3f](#)), leading to the trajectory of such dust particles being close to the orbit of C/2011 W3.

Analyzing the simulation results, we can get the initial pitch angles and reversal position of 10 nm dust particles. In [Figure 4a](#), the pitch angles are not near  $0^\circ/180^\circ$ , which means magnetic field geometry can effectively influence the dynamics of dust particles. In [Figure 4b](#), the heliocentric distance at time  $t_0$  represents the initial position of 10 nm dust particles. We can see that, although the initial positions are different, the reversal positions of the dust particles are similar and near  $2R_s$ . The particle with the smallest reversal heliocentric distance ( $1.86R_s$ ) is shown with the red line.

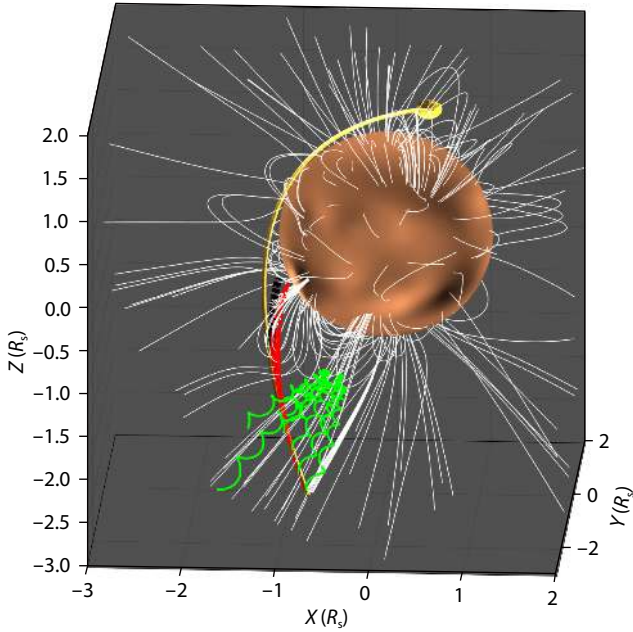


**Figure 2.** Trajectory simulation results of charged dust particles of different sizes. The sphere surface represents the magnetogram at an altitude of  $\sim 0.15R_s$  above the sun. The white lines and gold line denote the magnetic field lines and the orbit of C/2011 W3, respectively. The green lines, red lines and black lines represent the trajectories of different charged dust particles, the diameters of which are 10 nm, 1  $\mu\text{m}$  and 10  $\mu\text{m}$ , respectively.

This manifests that reversal of dust particles controlled by the magnetic mirror force can be one of the reasons for the formation of a dust-free zone. Dust particles with larger diameter are almost unaffected by the magnetic mirror force, but can undergo the process of decomposition and then become further charged to be more sensitive to the magnetic mirror force. Another possibility for the formation of the dust-free zone lies in dust sublimation and transformation to ions, which may enter into the dust-free zone to mix with solar coronal ions.

### 3.2 Dynamics of $\text{O}^{5+}$ Ions

We choose 32 different positions before the perihelion of C/2011 W3 as the  $\text{O}^{5+}$  ejection positions, with an interval of 1 minute in the time range between 2011-12-15 23:39 UT and 2011-12-16 00:10 UT. The initial position and initial velocity of the ions are assumed to be the same as that of the C/2011 W3. The charge-to-mass ratio of  $\text{O}^{5+}$  is

$$\frac{5}{16} \frac{e}{m_p}$$

Next, we can calculate the trajectory of  $\text{O}^{5+}$  released from multiple locations. The results displayed in Figure 5 show that the ions move along magnetic field lines in the open field region, and eventually away from the sun. When released in closed field regions, the ions bounce back and forth along the closed magnetic field lines. In Figure 6a, the initial pitch angles of  $\text{O}^{5+}$  at different releasing positions are also not near  $0^\circ/180^\circ$ , so the magnetic mirror effect can influence the motion of  $\text{O}^{5+}$ . According to Figure 5d,

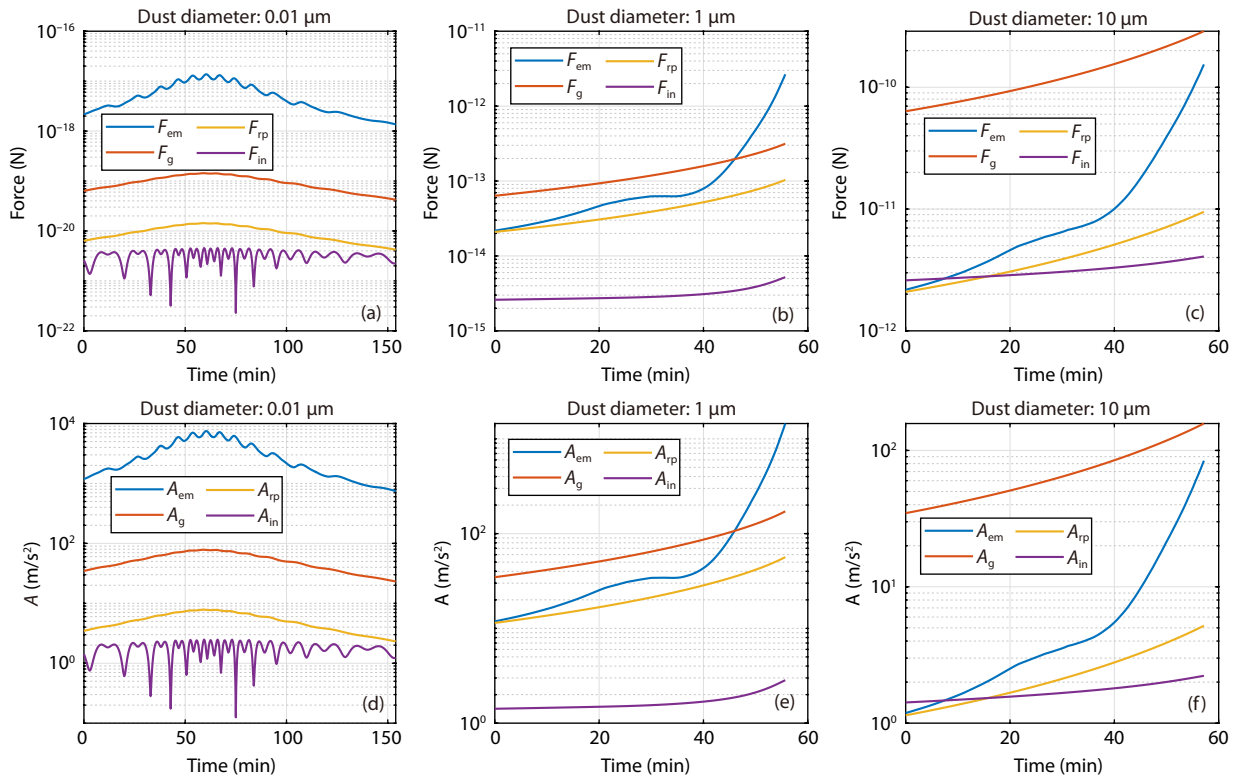


**Figure 3.** The comparison of different forces (top panels) and their corresponding accelerations (bottom panels) exerted on the dust particles of different diameters. For the  $0.01\mu\text{m}$  dust, the Lorentz force dominates the dust dynamics, whereas for  $1\mu\text{m}$  and  $10\mu\text{m}$  dust sizes, gravity dominates.

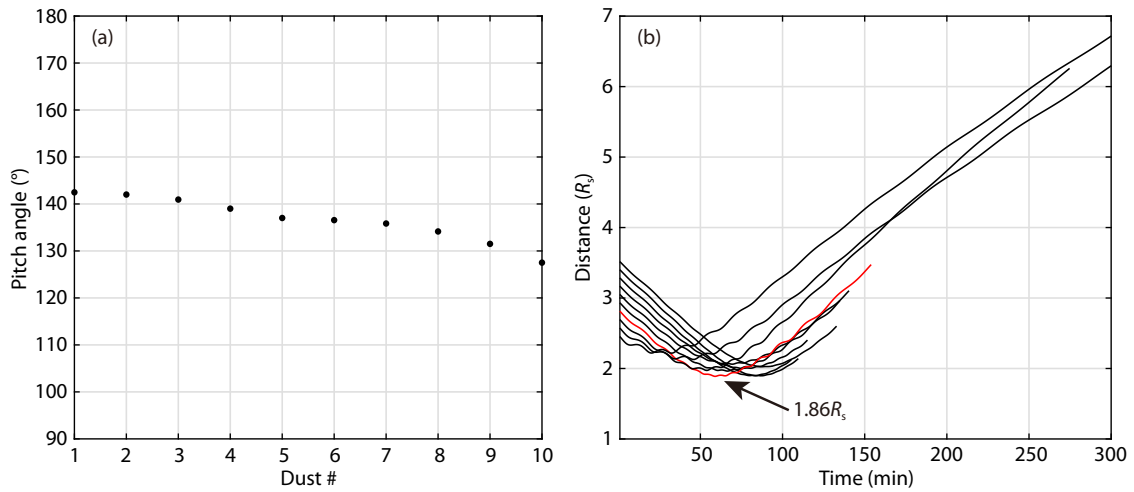


**Figure 4.** (a) The initial pitch angle of 10 nm charged dust particles. Dust # represents the sequence number of different release positions. (b) The change of heliocentric distance during the movement of 10 nm charged dust particles. The smallest heliocentric distance on the red line is  $1.86R_s$ .

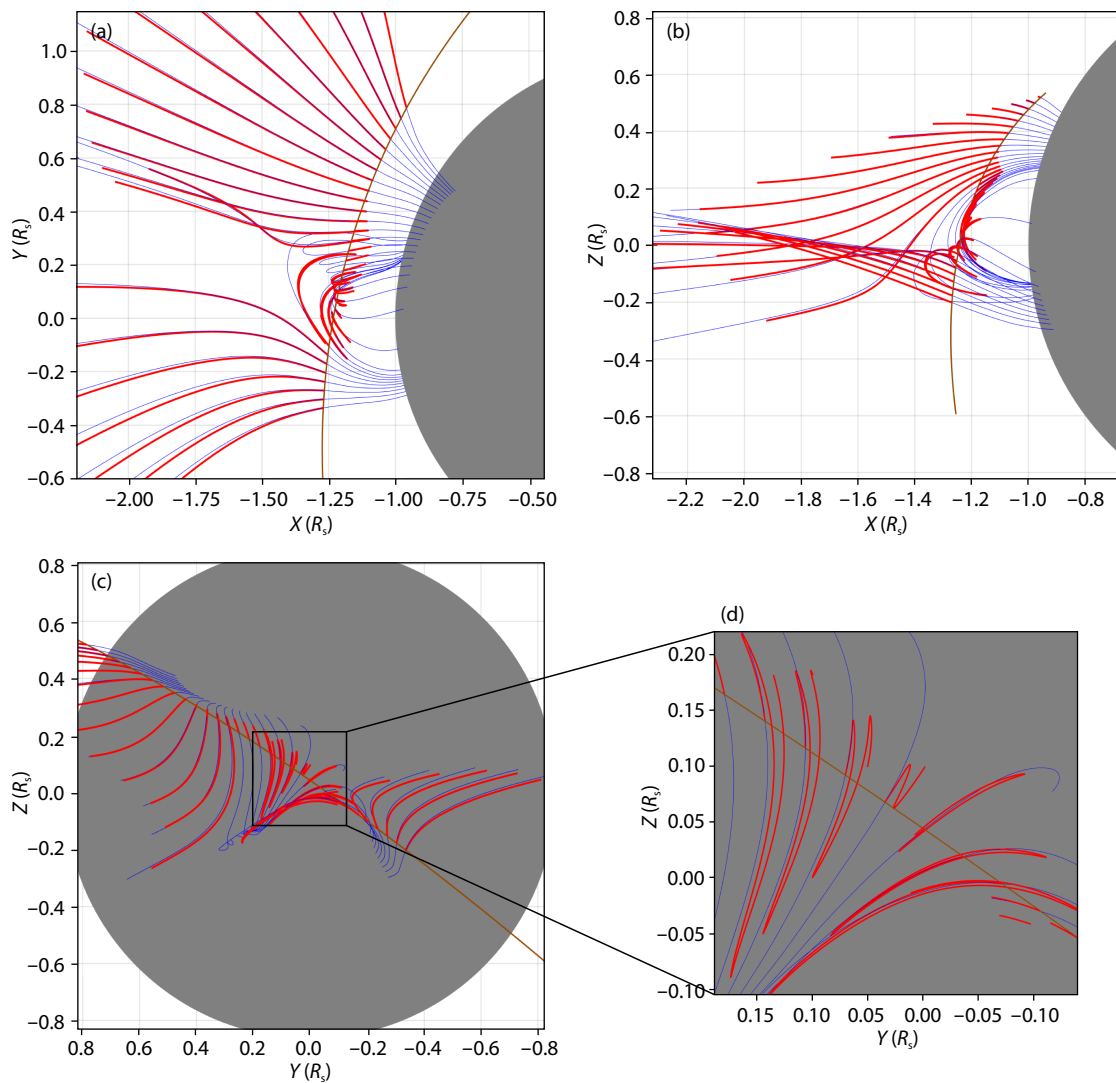


**Figure 5.** The trajectories (red lines) of  $O^{5+}$  at different release positions. The gray sphere, blue lines and brown line represent the solar surface, magnetic field lines and the orbit of C/2011 W3, respectively. Panels (a), (b), (c) illustrate the result from three different visual angles. (d) Zoom-in of the sub-region in (c) showing the drift motion of  $O^{5+}$ , which is much slower than the field-aligned movement.

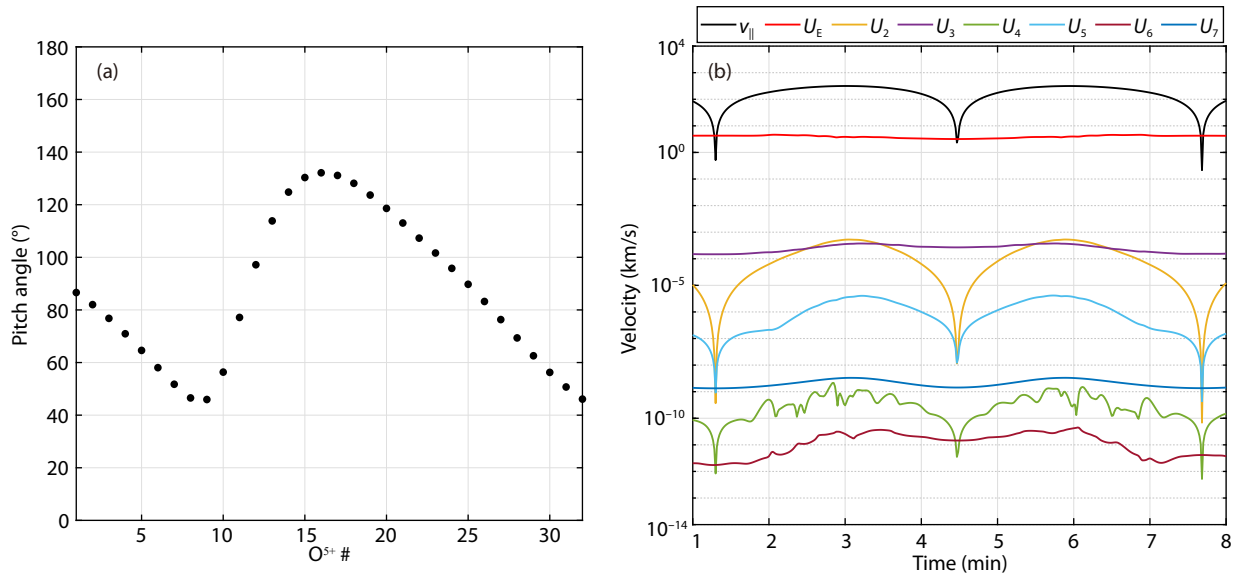


**Figure 6.** (a) The initial pitch angle of  $O^{5+}$ .  $O^{5+} \#$  represents the sequence number of different release positions. (b) A comparison of parallel velocity and different drift velocities of  $O^{5+}$  as released in close field regions. The variables with number subscripts in the legend correspond to the terms of the same order on the right side of Equation (6). For example,  $U_2$  corresponds to the second term of right side of Equation (6). The parallel velocity is much larger than the drift velocities, which are dominated by the  $\mathbf{E} \times \mathbf{B}$  drift.

the motion of ions along magnetic field lines is accompanied by the transverse motion perpendicular to the magnetic field lines. After comparing the contributions of each drift movement item (Figure 6b), we find that the electric field drift ( $\mathbf{E} \times \mathbf{B}$ ) dominates over other types of drift (e.g., magnetic curvature drift and magnetic gradient drift) and is the major contributor to vertical drift. We note that the vertical drift velocity is still far less than the parallel velocity even in the solar corona with a strong magnetic field (Figure 6b).

Although the initial velocity is the same as that of C/2011 W3, the direction of ions' motion is determined by both the comet's velocity and the direction of the magnetic field. As a result, when the direction of the magnetic field changes, so does the direction of the ions' movement. In observations, C/2011 W3 has a distorted tail (Downs et al., 2013); this is consistent with our simulation results. In addition, we find that the drift velocity of cometary ions is equal to the perpendicular velocity of the solar wind flow. Therefore, we suggest the perpendicular velocity of the solar wind in the solar corona inferred from cometary tail observations.

#### 4. Conclusions

Based on modeling data of the magnetic field and solar wind in the solar corona and inner heliosphere, we simulate the trajectories of charged dust particles and ions released from the comet C/2011 W3 at different locations, and analyze the particle movements. Dust particles with a diameter of 10 nm gyrate around the magnetic field lines when approaching the sun, and are finally rebounded away from the sun by the magnetic mirror force. We find that the smallest heliocentric distance of the rebound is  $1.86R_s$ . Thus, the magnetic mirror force is regarded as one of the reasons for the formation of the dust-free zone. Dust particles with larger size have smaller charge-to-mass ratio and are not easily controlled by the magnetic field due to the relatively smaller influ-

ence of electromagnetic force. When these large dust particles are fragmented into secondary nanometer-scale particles, the secondary particles can be again rebounded by the magnetic mirror force. Therefore, both the fragmentation of larger-diameter dust particles and the effect of the mirror force should be considered when estimating the boundary of the dust-free zone.

As for  $O^{5+}$ , it mainly moves along magnetic field lines, accompanied by the vertical drift motion (dominated by  $\mathbf{E} \times \mathbf{B}$  drift) perpendicular to the magnetic field line. After being released from C/2011 W3, the direction of tail ions' motion is determined by the directions of the comet velocity and magnetic field. Therefore, the distortion of the comet tail reflects the change of magnetic field directions. The striation tail is the result of particles moving along magnetic field lines, which is consistent with the observations in Downs et al. (2013) and McCauley et al. (2013). Local magnetic field distribution in the solar corona can be studied by observing the morphological evolution of a sun-grazing comet's tail. In addition, the transverse drift motion of ion particles may be used as a proxy for the transverse velocity of nascent solar wind at its source region.

This work is limited to the passive motion of charged particles in the context of the solar corona and solar wind without considering the feedback of charged particles to the nascent solar wind plasmas and electromagnetic fields. According to in-situ measurements in near-Earth space, interplanetary field enhancement (IFE) events are often observed and are suggested to be evidence of momentum transfer from solar wind to a dust cloud when the latter is accelerated and picked up by the former (Lai HR et al., 2015). The in-situ measurement of electromagnetic fields from Parker Solar Probe allows us to understand the features of dust in the inner heliosphere and corona (probably from sun-grazing comets) and the process of solar wind–corona coupling (Howard et al., 2019; Battams et al., 2020; Szalay et al., 2020). However, there is no

instrument to detect the dust particles directly on PSP, and measurements only provide indirect evidence for the dust and coupling (Page et al., 2020).

## Acknowledgments

The authors thank the Community Coordinated Modeling Center (CCMC) at Goddard Space Flight Center for providing the modeling data of the solar corona and inner heliosphere. The ephemeris of the comet C/2011 W3 is obtained from the JPL's Horizon database. This work is supported by NSFC under contracts No. 41874200 and 41421003, and supported by CNSA under contracts No. D020301 and D020302.

## References

- Battams, K., and Knight, M. M. (2017). SOHO comets: 20 years and 3000 objects later. *Philos. Trans. R. Soc. A Math. Phys. Eng. Sci.*, 375(2097), 20160257. <https://doi.org/10.1098/rsta.2016.0257>
- Battams, K., Knight, M. M., Kelley, M. S. P., Gallagher, B. M., Howard, R. A., and Stenborg, G. (2020). Parker solar probe observations of a dust trail in the orbit of (3200) Phaethon. *Astrophys. J. Suppl. Ser.*, 246(2), 64. <https://doi.org/10.3847/1538-4365/ab6c68>
- Bemporad, A., Poletto, G., Raymond, J. C., Biesecker, D. A., Marsden, B., Lamy, P., Ko, Y. K., and Uzzo, M. (2005). UVCS observation of Sungrazer C/2001 C2: possible comet fragmentation and plasma-dust interactions. *Astrophys. J.*, 620(1), 523–536. <https://doi.org/10.1086/427063>
- Biesecker, D. A., Lamy, P., Cyr, O. C. S., Llebaria, A., and Howard, R. A. (2002). Sungrazing comets discovered with the SOHO/LASCO coronagraphs 1996–1998. *Icarus*, 157(2), 323–348. <https://doi.org/10.1006/icar.2002.6827>
- Brueckner, G. E., Howard, R. A., Koomen, M. J., Korendyke, C. M., Michels, D. J., Moses, J. D., Socker, D. G., Dere, K. P., Lamy, P. L., ... Eyles, C. J. (1995). The large angle spectroscopic coronagraph (LASCO). In B. Fleck, et al. (Eds.), *The SOHO Mission* (pp. 357–402). Dordrecht: Springer. [https://doi.org/10.1007/978-94-009-0191-9\\_10](https://doi.org/10.1007/978-94-009-0191-9_10)
- Ciaravella, A., Raymond, J. C., and Giordano, S. (2010). Ultraviolet spectra of the C-2003k7 comet: evidence for dust sublimation in Si and C lines. *Astrophys. J.*, 713(1), L69–L73. <https://doi.org/10.1088/2041-8205/713/1/L69>
- Czechowski, A., and Mann, I. (2010). Formation and acceleration of Nano dust in the inner heliosphere. *Astrophys. J.*, 714(1), 89–99. <https://doi.org/10.1088/0004-637x/714/1/89>
- Dohnanyi, J. S. (1978). Particle dynamics. *Cosmic Dust*, 527–605. <https://ui.adsabs.harvard.edu/abs/1978codu.book..527D>
- Downs, C., Linker, J. A., Mikić, Z., Riley, P., Schrijver, C. J., and Saint-Hilaire, P. (2013). Probing the solar magnetic field with a Sun-grazing comet. *Science*, 340(6137), 1196–1199. <https://doi.org/10.1126/science.1236550>
- Giordano, S., Raymond, J. C., Lamy, P., Uzzo, M., and Dobrzycka, D. (2015). Probing the solar wind acceleration region with the Sun-grazing comet C/2002 S2. *Astrophys. J.*, 798(1), 47. <https://doi.org/10.1088/0004-637x/798/1/47>
- Gordovskiy, M., Browning, P. K., and Vekstein, G. E. (2010). Particle acceleration in a transient magnetic reconnection event. *Astron. Astrophys.*, 519, A21. <https://doi.org/10.1051/0004-6361/200913569>
- Howard, R. A., Vourlidas, A., Bothmer, V., Colaninno, R. C., DeForest, C. E., Gallagher, B., Hall, J. R., Hess, P., Higginson, A. K., ... Viall, N. M. (2019). Near-Sun observations of an F-corona decrease and K-corona fine structure. *Nature*, 576(7786), 232–236. <https://doi.org/10.1038/s41586-019-1807-x>
- Huang, T. S., Hill, T. W., and Wolf, R. A. (1988). Motion of charged particles in planetary magnetospheres with nonelectromagnetic forces. *J. Geophys. Res.: Space Phys.*, 93(A6), 5513–5523. <https://doi.org/10.1029/JA093iA06p05513>
- Ip, W. H., and Yan, T. H. (2012). Injection and acceleration of charged Nano-dust particles from sungrazing comets. *AIP Conf. Proc.*, 1436(1), 30–35. <https://doi.org/10.1063/1.4723586>
- Jessberger, E. K., Stephan, T., Rost, D., Arndt, P., Maetz, M., Stadermann, F. J., Brownlee, D. E., Bradley, J. P., and Kurat, G. (2001). Properties of interplanetary dust: information from collected samples. In E. Grün, et al. (Eds.), *Interplanetary Dust* (pp. 253–294). Berlin, Heidelberg: Springer. [https://doi.org/10.1007/978-3-642-56428-4\\_6](https://doi.org/10.1007/978-3-642-56428-4_6)
- Jewitt, D. (2012). The active asteroids. *Astron. J.*, 143(3), 66. <https://doi.org/10.1088/0004-6256/143/3/66>
- Jewitt, D., Li, J., and Agarwal, J. (2013). The dust tail of asteroid (3200) Phaethon. *Astrophys. J.*, 771(2), L36. <https://doi.org/10.1088/2041-8205/771/2/L36>
- Jia, Y. D., Russell, C. T., Liu, W., and Shou, Y. S. (2014). Multi-fluid model of a Sun-grazing comet in the rapidly ionizing, magnetized low corona. *Astrophys. J.*, 796(1), 42. <https://doi.org/10.1088/0004-637x/796/1/42>
- Jones, G. H., Knight, M. M., Battams, K., Boice, D. C., Brown, J., Giordano, S., Raymond, J., Snodgrass, C., Steckloff, J. K., ... McCauley, P. (2018). The science of sungrazers, sunskirters, and other near-sun comets. *Space Sci. Rev.*, 214(1), 20. <https://doi.org/10.1007/s11214-017-0446-5>
- Lai, H. R., Russell, C. T., Jia, Y. D., Wei, H. Y., and Angelopoulos, V. (2015). Momentum transfer from solar wind to interplanetary field enhancements inferred from magnetic field draping signatures. *Geophys. Res. Lett.*, 42(6), 1640–1645. <https://doi.org/10.1002/2015GL063302>
- Li, J., and Jewitt, D. (2013). Recurrent perihelion activity in (3200) Phaethon. *Astron. J.*, 145(6), 154. <https://doi.org/10.1088/0004-6256/145/6/154>
- Mann, I., Kimura, H., Biesecker, D. A., Tsurutani, B. T., Grün, E., McKibben, R. B., Liou, J. C., MacQueen, R. M., Mukai, T., ... Lamy, P. (2004). Dust near the Sun. *Space Sci. Rev.*, 110(3–4), 269–305. <https://doi.org/10.1023/B:SPAC.0000023440.82735.ba>
- McCauley, P. I., Saar, S. H., Raymond, J. C., Ko, Y. K., and Saint-Hilaire, P. (2013). Extreme-ultraviolet and X-Ray observations of comet Lovejoy (C/2011 W3) in the lower corona. *Astrophys. J.*, 768(2), 161. <https://doi.org/10.1088/0004-637x/768/2/161>
- Meyer-Vernet, M., Maksimovic, M., Czechowski, A., Mann, I., Zouganelis, I., Goetz, K., Kaiser, M. L., St. Cyr, O. C., Bougeret, J. L., and Bale, S. D. (2009). Dust detection by the wave instrument on STEREO: nanoparticles picked up by the solar wind?. *Sol. Phys.*, 256(1–2), 463–474. <https://doi.org/10.1007/s11207-009-9349-2>
- Mukai, T. (1981). On the charge distribution of interplanetary grains. *Astron. Astrophys.*, 99, 1–6.
- Page, B., Bale, S. D., Bonnell, J. W., Goetz, K., Goodrich, K., Harvey, P. R., Larsen, R., MacDowall, R. J., Malaspina, D. M., ... Szalay, J. R. (2020). Examining dust directionality with the parker solar probe FIELDS instrument. *Astrophys. J. Suppl. Ser.*, 246(2), 51. <https://doi.org/10.3847/1538-4365/ab5f6a>
- Raymond, J. C., McCauley, P. I., Cranmer, S. R., and Downs, C. (2014). The solar corona as probed by comet Lovejoy (C/2011 W3). *Astrophys. J.*, 788(2), 152. <https://doi.org/10.1088/0004-637x/788/2/152>
- Raymond, J. C., Downs, C., Knight, M. M., Battams, K., Giordano, S., and Rosati, R. (2018). Comet C/2011 W3 (Lovejoy) between 2 and 10 solar radii: physical parameters of the comet and the corona. *Astrophys. J.*, 858(1), 19. <https://doi.org/10.3847/1538-4357/aabade>
- Russell, H. N. (1929). On meteoric matter near the stars. *Astrophys. J.*, 69, 49. <https://doi.org/10.1086/143158>
- Sekanina, Z., and Chodas, P. W. (2007). Fragmentation hierarchy of bright sungrazing comets and the birth and orbital evolution of the Kreutz system. II. The case for cascading fragmentation. *Astrophys. J.*, 663(1), 657–676. <https://doi.org/10.1086/517490>
- Sekanina, Z., and Chodas, P. W. (2012). Comet C/2011 W3 (Lovejoy): orbit determination, outbursts, disintegration of nucleus, dust-tail morphology, and relationship to new cluster of bright sungrazers. *Astrophys. J.*, 757(2), 127. <https://doi.org/10.1088/0004-637x/757/2/127>
- Szalay, J. R., Pokorný, P., Bale, S. D., Christian, E. R., Goetz, K., Goodrich, K., Hill, M. E., Kuchner, M., Larsen, R., ... Schwadron, N. (2020). The near-sun dust environment: initial observations from parker solar probe. *Astrophys. J. Suppl. Ser.*, 246(2), 27. <https://doi.org/10.3847/1538-4365/ab50c1>
- Yang, L. P., Wang, L. H., He, J. S., Tu, C. Y., Zhang, S. H., Zhang, L., and Feng, X. S. (2014). Numerical simulation of superhalo electrons generated by magnetic reconnection in the solar wind source region. *Res. Astron. Astrophys.*, 15(3), 348–362. <https://doi.org/10.1088/1674-4527/15/3/005>